THE SPACEDRIVE PROJECT – MACH-EFFECT-THRUSTER EXPERIMENTS ON
HIGH-PRECISION BALANCES IN VACUUM

SPACE PROPULSION 2020+1
17 – 18 – 19 MARCH 2021

Maxime Monette[(1)], Matthias Kößling[(2)], Oliver Neunzig[(3)] and Martin Tajmar[(4)]

[(1)] *Institute of Aerospace Engineering, Technische Universität Dresden, Marschnerstrasse 32, 01307 Dresden, Germany, maxime.monette@tu-dresden.de*
[(2)] *Institute of Aerospace Engineering, Technische Universität Dresden, Marschnerstrasse 32, 01307 Dresden, Germany, matthias.koessling@tu-dresden.de*
[(3)] *Institute of Aerospace Engineering, Technische Universität Dresden, Marschnerstrasse 32, 01307 Dresden, Germany, oliver.neunzig@tu-dresden.de*
[(4)] *Institute of Aerospace Engineering, Technische Universität Dresden, Marschnerstrasse 32, 01307 Dresden, Germany, martin.tajmar@tu-dresden.de*

KEYWORDS: space propulsion, breakthrough propulsion, torsion balance, double-pendulum balance, Mach-Effect, Woodward thruster

ABSTRACT:

Concepts for propellantless space propulsion are carefully investigated using high-precision balances in the framework of the SpaceDrive Project. The Mach-Effect-Thruster, an original design from Woodward that relies on the particular vibration of an asymmetric, piezoelectric stack actuator to produce thrust, is one concept that was extensively tested. In an attempt to validate the results published in peer-reviewed literature, several MET devices were tested on two different types of balances in vacuum conditions: a torsion balance and an inverted counterbalanced double pendulum, as well as on a rotating apparatus. The instruments are characterized by background noise lower than 5 nN after averaging and are calibrated using laser interferometry and a voice coil with a high-resolution current source. Encased in grounded mu-metal shielding on the balance, and powered by dedicated amplifiers, the device was swept with a frequency between 20 and 50 kHz in order to identify the operating range with the largest beam deflections. Measurements with the torsion balance from a previous campaign seem to indicate vibration artefacts, thermal noise and changes in the experiment's centre of mass at specific resonance frequencies. These measurements were repeated with different device orientations on the double-pendulum balance, and deflections of similar magnitude that can be explained by thermal expansion and device resonance were also observed. Recording both balance beam displacements with a sampling rate of up to 25 MHz revealed a significant vibration when exciting the actuator around its longitudinal resonance, regardless of the mounting and isolation.

Calculations and simple modelling of the resulting pulsed force from the vibrations confirms the hypotheses made from balance measurements. Additional tests were performed on a rotating apparatus to investigate the presence of mass fluctuations in a centrifugal force field without having to synchronize with a push-pull force. Our tests reveal the presence of mechanical artefacts but no thrust.

1. INTRODUCTION

Woodward's Mach-Effect theory and experiments seem to support the claim of a new form of propellantless space propulsion that could revolutionize interstellar travel. In theory, the input of energy into a device through proper acceleration could create a mass fluctuation proportional to the rate of change of the power input [1]. That mass fluctuation could then be coupled to a synchronized push-pull mechanism to produce unidirectional thrust. The theory is based on Sciama's argument, that inertia is a result of the gravitational influence of distant matter in our universe [2], and it relies on the linearization of Einstein's field equations [3]. However, there are a few opponents to that theory disputing Woodward's derivation or proposing alternate derivations [4–7].

The embodiment of the theory is a multi-layered, piezoelectric stack pre-stressed between two different masses using a multiple screws connection, and is tested on a torsion balance in vacuum. The device is connected to the measuring apparatus by a bracket attached to its heavier end, and power is transferred to its electrodes using an amplifier. Precise torsion balance test results from Woodward have shown the presence of a particular force trace amounting up to 100 µN when the device is driven at a system resonance of 36 kHz and a power of about 30 W [8]. Allegedly, this effect was

consistently observed for the forward and reverse thrust-producing orientations, and was not observed when placing the thrust axis parallel to the torsion balance beam [1]. Other research teams, notably Buldrini et al. [9] and ourselves [10–13], have observed a similar effect in the forward runs at a much lower force level. The force trace is characterized by larger switching transients when turning the device on or off and by a smaller force, if any, during the pulse. In order to maximize the force and target the right operating conditions, we then performed different fixed frequency as well as swept frequency tests using separate sets of electronics. The results did not show much variation in amplitude [12]. Furthermore, force traces with the same magnitude were observed in all orientations, notably in the no-thrust producing axis. Also, the beam was shown to vibrate at lower frequencies when powering the test object and the effect was attributed to vibrational and thermal artefacts [12,13].

In order to better explain the origin of the effects observed, a different force measuring apparatus was conceived and tested. The inverted counterbalanced double-pendulum, or double-pendulum balance (DPB), was constructed to reduce the pseudo-forces observed coming from centre-of-mass shifts on the thruster plane. Indeed, thermal expansion of different parts of the test object can lead to a detectable beam displacement on the torsion balance that can be mistaken for thrust. The double-pendulum balance is composed of two horizontal planes resting on three aluminium beams and the thruster is placed on the top plane. The linear deflection of the frame due to a thrust force is supported by nine linear torsional springs. Due to the particular configuration and increased stability of the structure, centre-of-mass shifts occurring on one horizontal plane itself should not lead to any detectable frame displacement. In section 2, the measuring apparatus and test devices will be described in detail and characterized. The test results on the different balances will be examined and compared in order to draw our conclusions in section 3.

Lastly, a different concept for detecting mass fluctuations that does not require the generation of thrust, or a sensitive thrust balance, was examined. A similar pre-stressed, piezoelectric actuator with an embedded passive piezo-disk was attached to an arm and spun at varying angular frequency. The goal was to observe the influence of the energy input on the centrifugal force measurement by the passive gauge. This experiment, also conceived by Woodward [14], was meant to simplify the detection of mass fluctuations at twice the driving signal frequency. This concept will be thoroughly investigated in section 4.

2. EXPERIMENTAL SETUP

2.1. Thrust balances

Understanding the functioning of the measuring instrument is a crucial part of the investigation. The mechanism of the well-known torsion balance is described in Figure 1. A force in the balance plane, perpendicular to the balance beam, will generate a displacement that will be detected at the other end by a laser interferometer (attocube, IDS3010). The laser has a resolution of 1 pm and a noise of 2 nm at room temperature in medium vacuum where the experiments are performed. Power to the test object is transmitted through liquid metal contacts in the pivot axis, as can be seen in the CAD model, to allow the free rotation of the beam and exclude forces from rigid cables. The balance is calibrated with small pulses in a range of 1 to 100 µN using a voice coil mounted in the thrust axis. The balance was also calibrated by voice coils mounted in the two other axes and the tests showed no important force [10]. However, centre of mass shifts in any axis could create some balance beam zeroing, which hasn't been characterized yet.

The double-pendulum balance relies on the unstable equilibrium of the upper platform with respect to the balance's centre of gravity and its connection to the bottom platform, where the displacement is measured. The upper platform, where the test device is mounted, is supported by three axes and the whole frame is supported by a total of nine C-flex torsional springs. The balance's frame and parallelogram deflection can be seen in Figure 2. This balance also uses the laser interferometer from attocube and the voice coil for calibration. Sorbothane pads separate the test device from the support platform to damp vibration. The sensitivity of the balance can be changed by adding weights on the lower platform, or by shifting weights on the platform's supporting. Twisting the frame seen in the picture would result in a displacement of the upper platform as well. However, the frame is resistant to the centre-of-mass shifts occurring on one horizontal plane. Both balances use passive eddy current damping: a permanent magnet is moved between two adjustable copper plates. Damping is used to limit excessive and transient displacements in order to measure steady thrust. Whereas the torsion balance (TB) has the magnet on the moving beam to limit the effects of electromagnetic interaction with the device, the double-pendulum balance has its permanent magnet connected to the supporting structure across the lower platform, since the electronics are located far from it. This balance also features liquid contacts for power transmission, aligned along one side of the structure and featuring pins dipped in Galinstan cups, to remove any force from connecting rigid cables.

Calibration using a set of known forces from the voice-coil reveals a linear correlation on the left of Figure 3 for both balances. The slope of the interpolation represents the calibration factor of the balances, indicating the slightly higher sensitivity of the torsion balance in this configuration. Shorter calibrations are performed before and after each thruster test sequence. Then, the balance response to a 1 µN, 20 s pulse from the voice coil, illustrated on the right-hand side of Figure 3, shows a slightly underdamped curve and a very similar damping ratio for both balances. This response is known to represent the simple harmonic oscillator response. The force of the voice coil is accurately measured using our previously measured calibration factor and the time response is around 6 s for both balances. Thus, the test pulses were selected to be slightly longer.

2.2. MET and electronics

The embodiment of the Mach-effect theory is illustrated in Figure 4, showing the screw connection, the bracket, the piezoelectric stack actuator sandwiched between an aluminium and a brass mass. Energy input to the piezoelectric actuator is performed using a dedicated amplifier (PA04 in bridge-mode, APEX). The whole system is shown in the diagram of Figure 5. The amplifier was chosen to deliver the desired voltage, by-passing the need for a transformer and audio amplifier as used by Woodward [15]. Not only was it shown that the piezo-amplifier is less subjected to noise, the force trace observed was also similar to using the audio amplifier and transformer [12].

The piezoelectric device was characterized using its embedded, passive strain gauge as well as the impedance by sweeping the driving frequency and examining the signals. In Figure 6, left, the impedance spectra were obtained for the two devices at different times of the campaign and indicate the resonances (peaks) and the anti-resonances (troughs). The second curve of the WT3 device indicates the influence of a depolarization event that occurred sometime during our campaign. This suggests that the mechanical properties of some of the piezo-discs were modified, probably due to mechanical stresses during repeated testing under harsh conditions or an inaccurate retightening of the bolt. In Figure 6, right, the gauge signal to the input voltage reveal the same resonances as illustrated in the previous graph: an important realization is that the passive gauge shows the same resonances as in the impedance spectrum. The two devices tested, NS5 on the torsion balance and WT3 after depolarization event, on the double-pendulum balance, were obtained from Woodward and show different resonances. The balance test runs were performed by paying attention to the properties of the devices as detected by spectral analysis. Fixed frequency pulses of 16 s, where the driving frequency is held

constant, as well as 24 s forward driving frequency sweeps, and a minimum of 5 runs in each orientation were performed on each balance. The operation included a reasonable cool-down period to limit device overheating.

2.3. Rotary device

This apparatus relies on a simpler principle to detect the mass fluctuation than a torsion balance. As the piezoelectric stack is rotated, the centrifugal force acting on the embedded strain gauge will vary if the mass of the stack varies due to the Mach-effect. The strain gauge is simply a thin, passive PZT disk. The challenge of this setup is to reduce electromagnetic interaction, and noise in the strain gauge signal. As portrayed in Figure 7, the stack is connected to a 8.4 cm long arm and can be rotated to 60 Hz by a DC brush motor (Johnson Electric, HCP877-011P). This rotation speed, measured using a photoelectric barrier and oscilloscope, results in a stack acceleration of 1100 **g.** The power is transmitted using a slip-ring (Senring, G012-12) with a maximal voltage capacity of 440 VAC. The same amplifier electronics are used as for the balance tests and are assembled as shown on the right side of Figure 7. The spectrum and calibration of the embedded gauge for an accurate determination of the centrifugal force are discussed in section 4. Lastly, since the mass fluctuations are expected at twice the driving frequency, an 8th order Butterworth high-pass filter was used to filter the first harmonic component of the gauge signal and extract the second harmonic component.

3. BALANCE TESTS

Characterization of the balance started with running DC current over a resistor to analyse electromagnetic interaction and thermal effects. Figure 8, left, shows the results of both balances when driving a 15Ω resistor with 1.5 A for the double-pendulum balance and 0.8 A for the torsion balance. In the latter case, the test resulted in a small but noticeable thermal drift of about 30 nN between the start and end of the pulse. This kind of linear thermal drift can be filtered and is not a thrust force. However, one notices a major discrepancy between the two tests that cannot be simply explained by the difference in the currents. In the case of the double-pendulum balance, the overall force response was significantly larger, with a drift of around 1.5 µN and a superposed, steady force of around 1 µN. This effect was investigated after the MET test campaign, and was attributed to the repulsion force between the Galinstan liquid and the immersed pin contacts. However, since the experiments conducted with the MET are exclusively performed using AC signals, these DC current effects can be ignored.

Then, the sinusoidal pulse test with the voice coil resulted in comparable force responses for both

3

balances, as seen on the right-hand side of Figure 8. With a repetition rate of 0.5 Hz, switching transients just below 100 nN in magnitude can be observed, as well as a low amplitude 0.5 Hz oscillation. The amplitude of the oscillation is expected to go down with increasing excitation frequency, however, the current source (Keithley 2450) could not be driven at higher frequencies. Moreover, the noise seen in the torsion balance profile is greater than on the double-pendulum balance, which correlates with the latter's higher force-displacement conversion factor, given similar background building noise. This test shows that both balances can be considered to behave like a simple harmonic oscillator, and that larger switching transients may appear due to low frequency excitation.

For the fixed frequency test with the MET, care was taken to pick the frequency with the highest potential effect, chosen to be at the loaded system's resonance, in our case, the device's resonance. In the torsion balance's case, this occurred at 34.0 kHz with the NS5 device and for the double-pendulum balance at around 21.8 kHz for the partially depolarized WT3 device (see Figure 6). The force traces are examined without first going into the detail of the potential electromechanical phenomena that depend on the health of the piezoelectric devices between the tests. Starting with the 0°, or forward, orientation in Figure 9, left, it is obvious that the electromechanical behaviour is different between the two sets of runs, as seen from the current traces. Whereas the current amplitude during the double-pendulum test is constant at 0.45 A, the amplitude for the torsion balance test has a 0.65 A spike at the beginning before dropping rapidly to 0.48 A, and experiences a slow rise until the end of the profile. In both cases, though, both currents can be turned on and off almost instantaneously. Interestingly, the force traces are almost identical, even if offset by about 50 nN, despite the difference in devices, current and frequency. Both force traces show the same behaviour: low noise before turn-on, a positive switch-on transient, a recoil of the balance in the opposite direction during the pulse, then a slow return to the zero-line and finally a sharp negative switch-off transient. In the 90° case, on the right of Figure 9, the device is parallel to the balance beam. Again, the current behaviour is slightly different, even though the same respective frequencies were selected. This time, the current is higher, with a starting current of 1.1 A for NS5 on the torsion balance, and device WT3 stays at 0.45 A on the double-pendulum balance.

In the torsion balance profile, one observes the same force trace as for the 0° orientation, only with the now smaller switching transients in the opposite direction. The double-pendulum profile also shows a small switching transient at turn-on but the force shoots up and reaches 80 nN and does not show an important switch-off transient. This result does not seem consistent with the theory of unidirectional thrust.

In the sweep frequency tests, the force traces for the 0° and 90° orientations are plotted for each balance alongside the driving frequency and the current against time. Here, the sweeps were conducted with the partially depolarized WT3 device on both balances. Figure 10, left, shows the force profiles for both orientations for the double-pendulum, with linear correction for thermal drift. In the 0° case, there is a sharp force peak which occurs at the first resonance around 22 kHz, demonstrated by the current peak. In the 90° case, the behaviour is very similar, only the transient force is smaller and occurs at a slightly higher frequency. Notice that there are no switching transients at the beginning or end of the sweeps, but rather slower drifts. Figure 10, right, shows the same graph for the torsion balance with linear thermal drift correction, where sharp force peaks of a few 100 nN can be seen. The transient force seems to occur at the first resonance, for the 0° orientation, and it is exactly reversed for the 90°, at the second resonance. Since the magnitude of the effects is similar for both orientations, these observations hint at something other than thrust.

Hence, the displacement of the beam of both balances was observed using the laser interferometer with high sampling frequency. Figure 11, left, depicts the result of a single waveform, discrete Fourier transform (DFT) when driving the device around the same frequency as for the previous, respective fixed frequency tests. In the frequency spectrum, the driving frequencies are not to be seen, however, two obvious peaks are present: 500 Hz for the torsion balance and close to 900 Hz for the double-pendulum, along with other lower frequency peaks. These vibrations were only observed around the resonances of the system when powering the device, as can be seen in Figure 11, right, where the amplitude of these lower range frequency vibrations is plotted. In the case of the double-pendulum, the amplitude of the vibration is lower and consistent so far with the other balance tests and higher force-displacement conversion factor. Although the exact cause of these sub-harmonic vibrations is unknown, it's reasonable to assume that one or more components of the complex assembly are excited by the device's amplified oscillations at resonance. How oscillating forces can cause either balance to show switching transients has already been extensively examined by us using the voice coil [13].

4. ROTARY DEVICE TESTS

The rotary device has the advantage of looking at the mass fluctuation without the need of a complex thrust balance, and also without having to synchronize the device's first harmonic oscillations with electrostriction to produce thrust, required according to Woodward and Fearn [15]. Knowing the voltage-force conversion constant of the passive gauge embedded in the stack allows one to determine the change in the forces from the gauge signal. Using the piezoelectric voltage coefficient (g_{33}) of about 25 Vm/N for hard PZT materials, the conversion factor for the 0.3 mm thick piezodisk should be 26.5 mV/N [16]. However, this will be different when placed in a pre-stressed multi-layered stack with screw connection. Thus, the stack was put to test using an electromechanical, universal testing machine (ElectroPuls, E3000). The results of the calibration using a 100 N pulling force at varying forcing frequency, and a constant pre-stress of 200 N in addition to the pre-stress of the bolts, are shown in Figure 12. The curve shows a stabilization around 22 mV/N, which is close to the prediction and means that the external force is well transmitted to the strain gauge and the stack is stiffer than the parallel screw connection. Below a forcing frequency of 50 Hz, the conversion factor is lower since the small piezoelectric charge has time to dissipate before the next pulse. On one hand, it seems that the conversion factor reaches a steady value at higher frequencies, and it is assumed that it will not change for high frequencies in the kHz range. Also, an internal force generated in the pre-stressed assembly by charging the piezoelectric stack could result in different dynamics compared to the external pulling force used in the calibration method. Therefore, an additional calibration method will be developed in the future to verify these assumptions.

In Figure 13, the graph on the left illustrates a frequency spectrum of the gauge signal amplitude against the driving frequency for a constant AC voltage input of 180V amplitude applied to the stack in a range of 10 to 45 kHz. The values are obtained by extracting the main component from a DFT of the unfiltered gauge signal waveforms in response to each excitation frequency. Furthermore, the three curves are obtained at different rotation rates of the apparatus. If the voltage-force conversion factor of the passive gauge remains constant over the frequency range, one can accurately determine the internal force acting on the gauge at any frequency. In addition, the centrifugal force can be ignored since it is a constant force if the rotation rate is held fixed throughout the test run during which the AC signal is applied. Hence, the 0 rpm curve strictly shows the internal forces, varying with the driving frequency around resonances, as expected.

In the event that the frequency response of the stack does not depend on the rotation rate, the mass fluctuation could be obtained as the difference in the second harmonic amplitudes extracted from the gauge signal, since the mass fluctuation is expected to occur at twice the driving frequency. However, Figure 13, left, shows that the internal forces do vary with the rotation rate, especially in the neighbourhood of the resonance and anti-resonance peaks. The analysis could focus on the minimal difference between the 1800 and 3600 rpm curves, but the discrepancy is still too large compared to the predicted mass fluctuation.

Figure 13, right, shows the second harmonic component of the gauge signal during the driving frequency sweep, at various rotation rates, obtained this time from a DFT analysis of the filtered gauge signal. This figure shows that there is an important non-linearity present around the resonances, even without rotation, as detected from the 0 rpm curve. Moreover, there is an important difference in the second harmonic component for the varying rotation rates. Is this difference due to the Machian mass fluctuation? Not necessarily. Since the first harmonic component of the internal forces do vary with the rotation rate, so could the second harmonic component vary as well. Since the exact nature and distribution of the nonlinearity present in the stack cannot be accurately determined, the mass fluctuation, if present, is hidden in the second harmonic content of the piezoelectric oscillation. The solution to this problem requires a re-design of the test object to remove even the smallest nonlinearity, and an accurate quantitative analysis demands a re-evaluation of the calibration method, which are both on-going.

5. CONCLUSION

The exciting perspective of a new form of propellantless thrust has led to a thorough investigation of the claim for Mach-Effects. The results obtained for MET tests with a sub-μN torsion balance in the framework of the SpaceDrive project have been corroborated by the results obtained with the double-pendulum thrust balance. Both balances seem to suffer the same weakness in measuring the force transmitted by a piezoelectric stack: they rely on mechanical connections susceptible to vibration. Since effects of the same magnitude were observed for both thrust-producing (0°) and non-thrust producing (90°) orientations of the device, an investigation of possible artefacts was undertaken. Examining the movement of balance beams using a laser interferometer with high sampling frequency led to the discovery of vibrations at frequency lower than the driving frequency, especially at resonant excitation. Comparing the results with the known and tested response of harmonic oscillators to a sinusoidal excitation provides an explanation for the switching transients observed. Lastly, the nature and magnitude of the force traces observed seem to be relatively indifferent to the change in the thrust balances, electronics, devices, currents and driving

frequencies. Thus, it is concluded that the claimed thrusts using an MET or MEGA thruster device consist in vibrational artefacts.

Furthermore, first tests with a rotary device to detect Machian- or mass fluctuations of other nature have been performed. Our results have been limited by the nonlinearity present in the piezoelectric stacks, which will be improved in future tests

7. REFERENCES

1. Woodward, J.F. *Making Starships and Stargates: The Science of Interstellar Transport and Absurdly Benign Wormholes*; Springer: New York, 2013; ISBN 9781461456223.
2. Sciama, D. *On the Origin of Inertia*; Cambridge, 1953.
3. Woodward, J.F. Flux capacitors and the origin of inertia. *Found. Phys.* **2004**, *34*, 1475–1514.
4. Rodal, J.J.A. A Machian wave effect in conformal , scalar – tensor gravitational theory. *Gen. Relativ. Gravit.* **2019**, *51*, 1–23.
5. Williams, L.L.; Inan, N. Maxwellian mirages in general relativity Available online: http://arxiv.org/abs/2012.08077.
6. Brans, C.H. Absence of inertial induction in general relativity. *Phys. Rev. Lett.* **1977**, *39*, 856–857.
7. Fearn, H.; Rossum, N. van; Wanser, K.; Woodward, J.F. Theory of a Mach Effect Thruster II. *J. Mod. Phys.* **2015**, *06*, 1868–1880.
8. Woodward, J.F.; Kennifick, D.; Broyles, M.; Akins, C.; Fearn, H.; Rodal, J.; March, P. *Mach Effects for In-Space Propulsion: Interstellar Mission - NIAC Phase II Final Report*; Los Angeles, 2020;
9. Buldrini, N.; Tajmar, M.; Marhold, K.; Seifert, B. Experimental Results of the Woodward Effect on a uN Thrust Balance. In Proceedings of the AIAA/ASME/SAE/ASEE Joint Propulsion Conference & Exhibit; 2006; Vol. 42, pp. 1–12.
10. Kößling, M.; Monette, M.; Weikert, M.; Tajmar, M. The SpaceDrive project - Thrust balance development and new measurements of the Mach-Effect and EMDrive Thrusters. *Acta Astronaut.* **2019**, *161*, 139–152.
11. Tajmar, M.; Kößling, M.; Weikert, M.; Monette, M. The SpaceDrive Project - First Results on EMDrive and Mach-Effect Thrusters. **2018**.
12. Monette, M.; Kößling, M.; Tajmar, M. The SpaceDrive Project - Progress in the Investigation of the Mach-Effect-Thruster Experiment. In Proceedings of the 36th International Electric Propulsion Conference; 2019; pp. 15–20.
13. Monette, M.; Kößling, M.; Neunzig, O.; Tajmar, K. Experimental Investigation of Mach-Effect Thrusters on Torsion Balances. *Acta Astronaut.* Submitted: **2021**.
14. Woodward, J.F. A Test for the Existence of Mach Effects With a Rotary Device. In Proceedings of the AIP Conference Proceedings 1208; 2010; pp. 227–236.
15. Fearn, H.; Woodward, J.F. New Experimental Results of the Mach Effect Gravitational Assist (MEGA) Drive. In Proceedings of the AIAA Propulsion and Energy Forum NNF; Indianapolis, 2019; pp. 1–12.
16. PI Ceramic GmbH Material Data Available online: https://www.piceramic.com/en/products/piezoelectric-materials/#c15193.
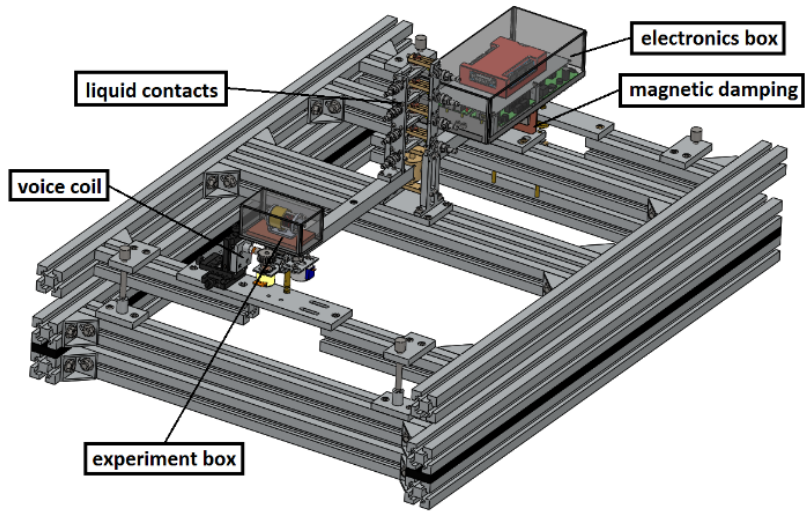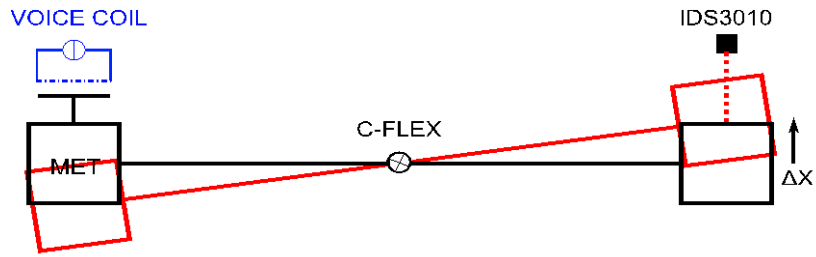
Figure 1: sketch (top) and CAD (bottom) of the torsion balance
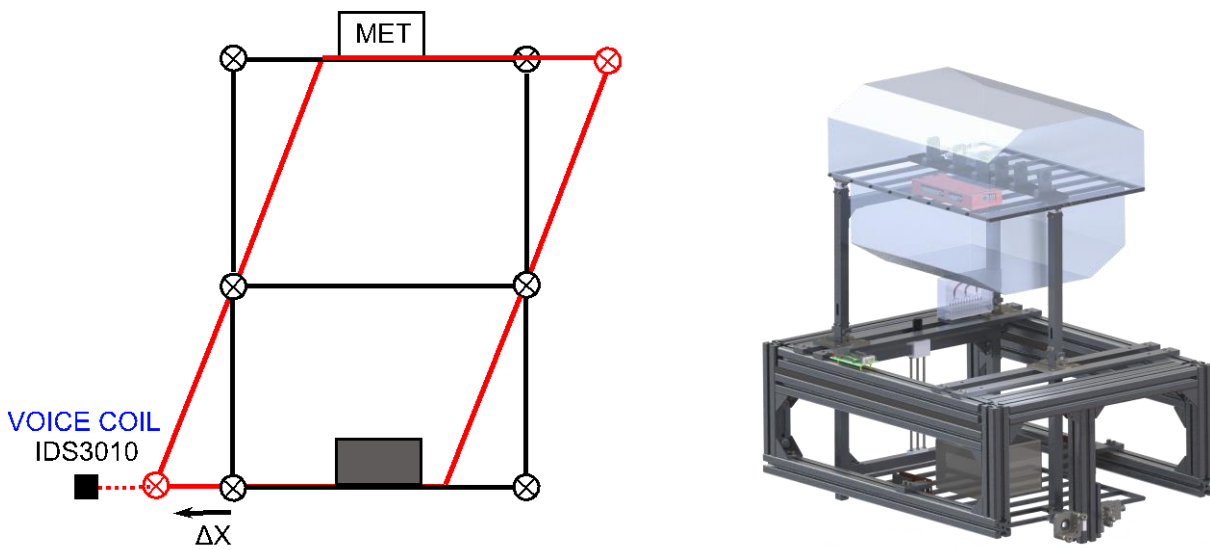
Figure 2: sketch (left) and CAD (right) of the double-pendulum balance
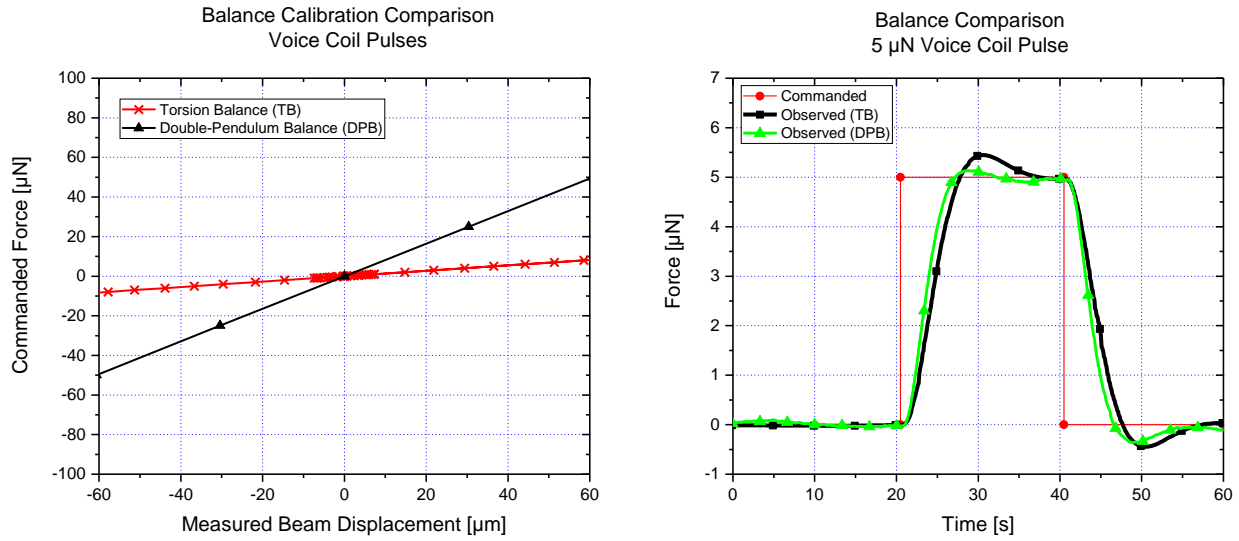
Figure 3: calibration comparison
Left: full calibration, both balances, right: single pulse calibration, both balances

Figure 4: picture of the MET
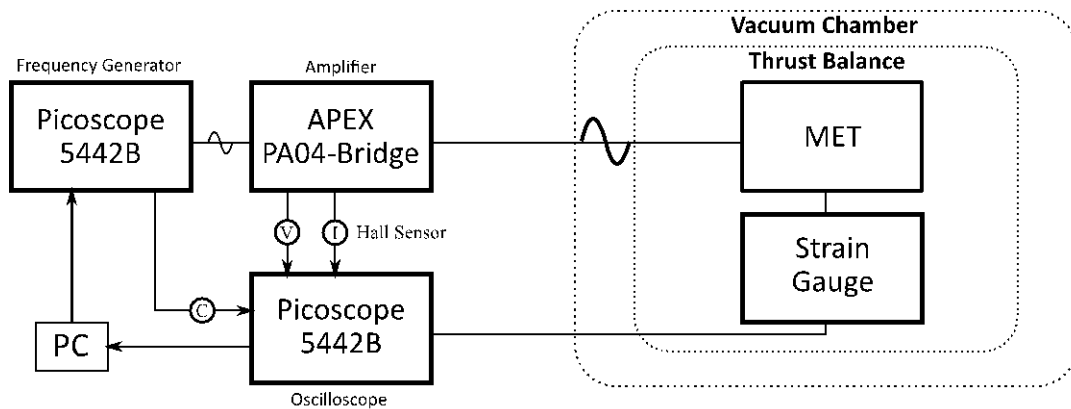
Figure 5: electronics diagram
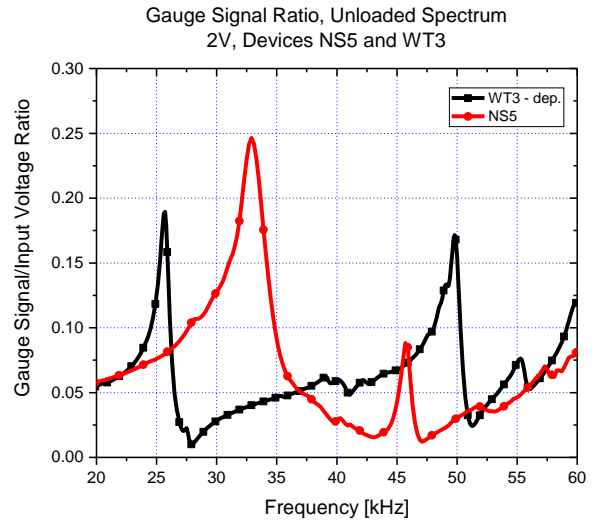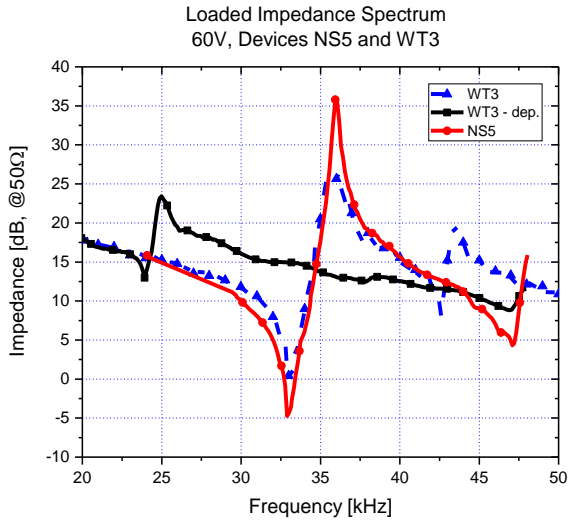
Figure 6: spectrum of devices, at different times
Left: impedance spectrum, right: gauge signal spectrum
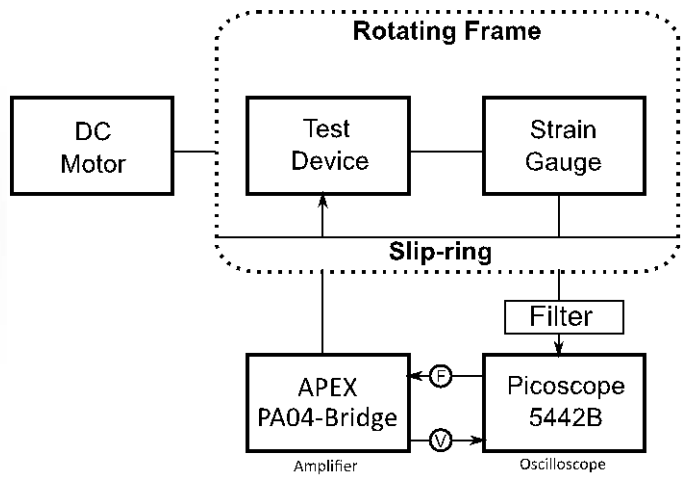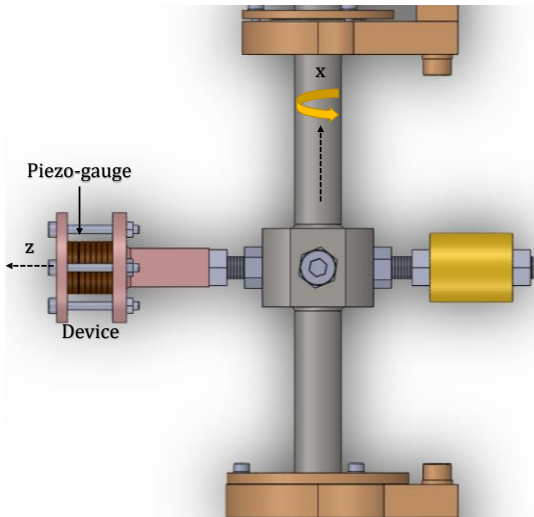
Figure 7: rotary apparatus setup
Left: CAD model, right: electronics diagram
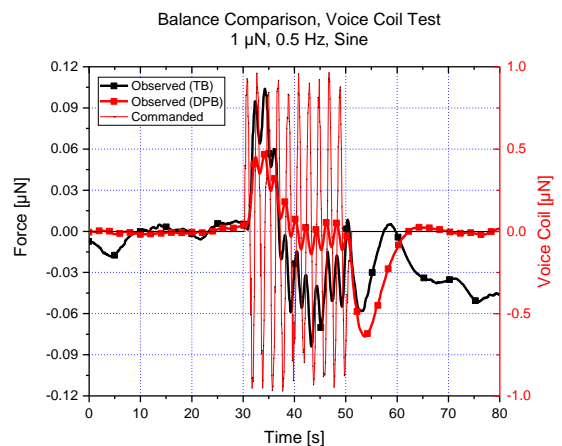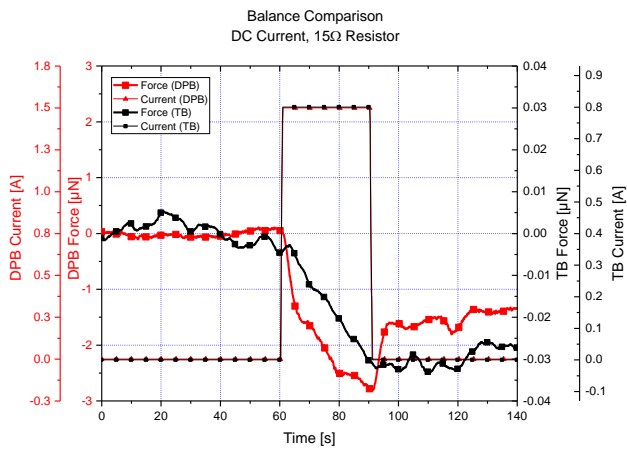
Figure 8: zero tests
Left: DC current test, right: voice coil sine test

9
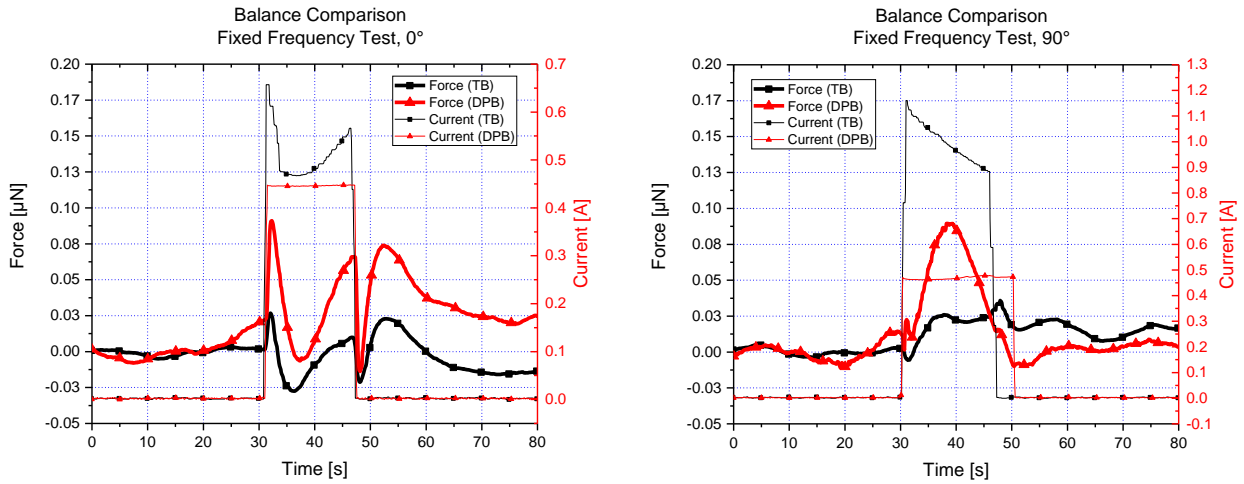
Figure 9: MET fixed frequency balance tests
Left: 0° orientation, right: 90° orientation
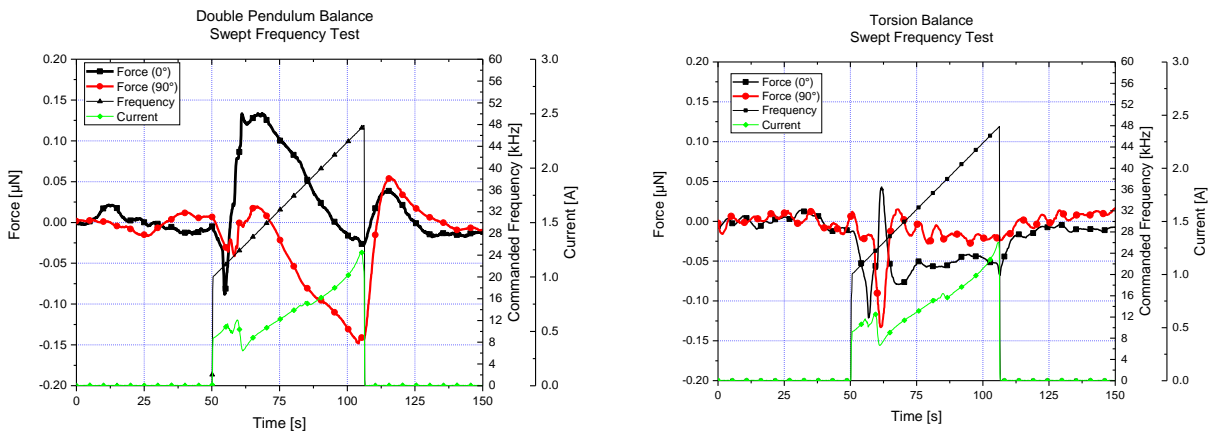
Figure 10: MET sweep balance tests
Left: torsion balance sweep, right: double pendulum balance sweep
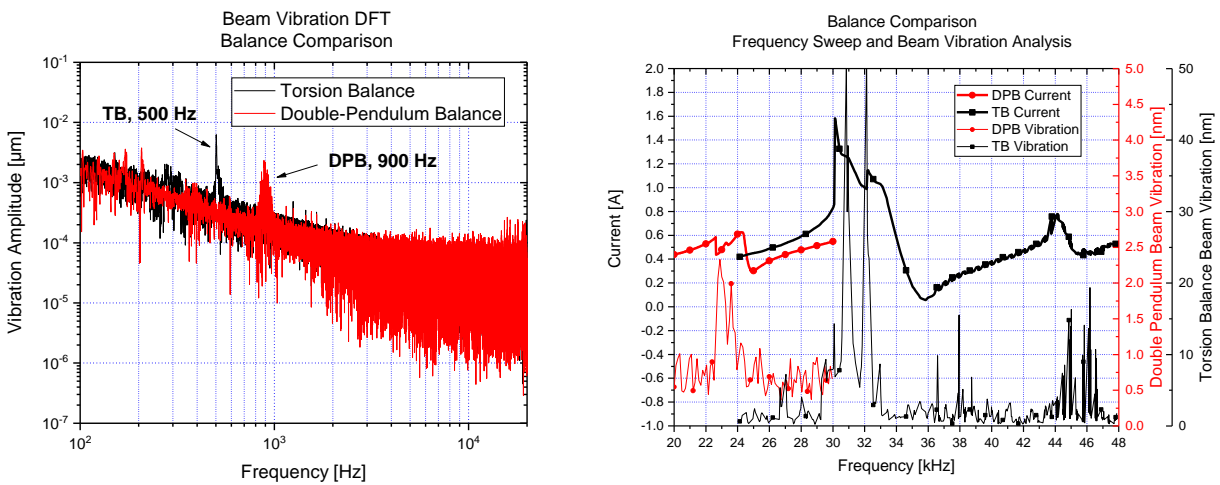
Figure 11: MET beam vibration analysis
Left: DFT, one waveform, both balances, right: 90° sweep, both balances

10
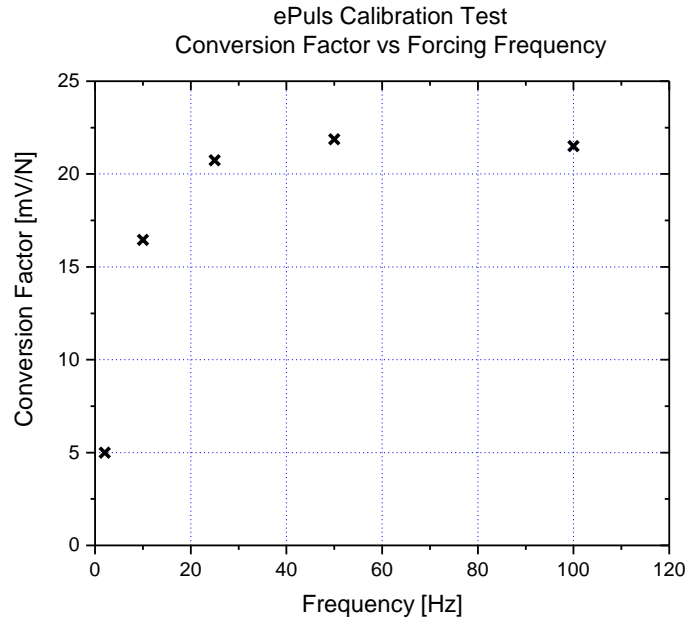
Figure 12: ElectroPuls calibration
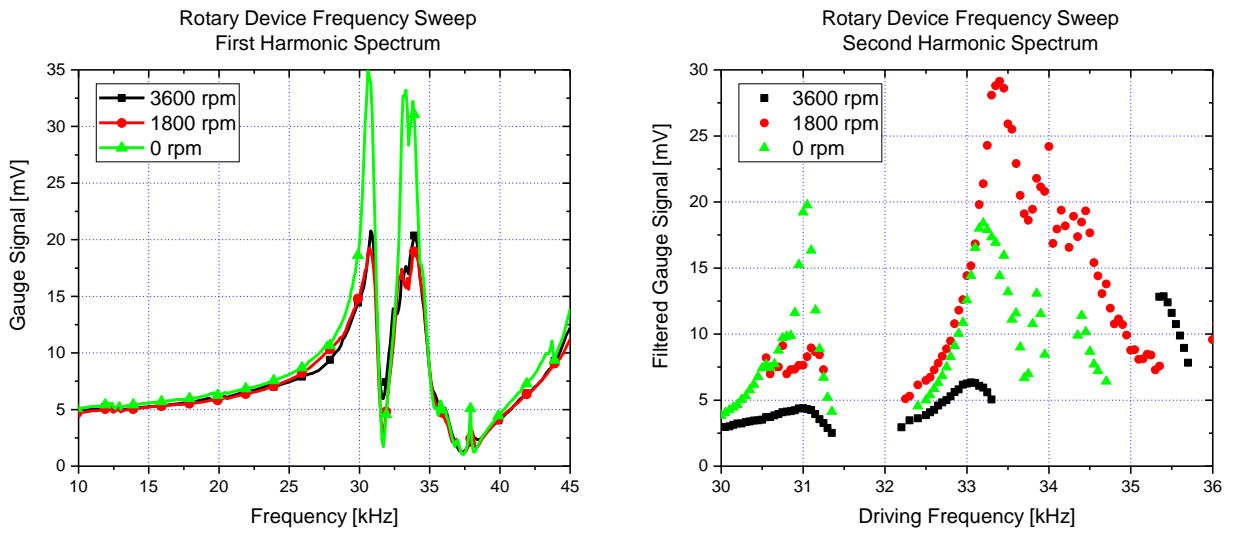
Figure 13: S03 device spectra vs rotation rate
Left: first harmonic spectrum, right: second harmonic spectrum.